



Surface passivation of germanium by atomic layer deposited Al₂O₃ nanolayers

Wilhelmus J. H. Berghuis^{1,a)} , Jimmy Melskens¹, Bart Macco¹, Roel J. Theeuwes¹, Marcel A. Verheijen^{1,2}, Wilhelmus M. M. Kessels^{1,a)}

¹Eindhoven University of Technology, Postbus 513, 5600 MB Eindhoven, The Netherlands

²Eurofins Materials Science BV, High Tech Campus 11, 5656 AE Eindhoven, The Netherlands

^{a)}Address all correspondence to these authors. e-mails: w.j.h.berghuis@tue.nl; w.m.m.kessels@tue.nl

Received: 14 September 2020; accepted: 30 November 2020; published online: 28 January 2021

Surfaces of semiconductors are notorious for the presence of electronic defects such that passivation approaches are required for optimal performance of (opto)electronic devices. For Ge, thin films of Al₂O₃ prepared by atomic layer deposition (ALD) can induce surface passivation; however, no extensive study on the effect of the Al₂O₃ process parameters has been reported. In this work we have investigated the influence of the Al₂O₃ thickness (1–44 nm), substrate temperature (50–350 °C), and post-deposition anneal (in N₂, up to 600 °C). We demonstrated that an effective surface recombination velocity as low as 170 cm s⁻¹ can be achieved. The role of the GeO_x interlayer as well as the presence of interface charges was addressed and a fixed charge density $Q_f = -(1.8 \pm 0.5) \times 10^{12} \text{ cm}^{-2}$ has been found. The similarities and differences between the passivation of Ge and Si surfaces by ALD Al₂O₃ prepared under the same conditions are discussed.

Introduction

Germanium (Ge) is a versatile semiconductor which currently attracts attention in several research fields. In microelectronics for example, it is considered one of the most attractive alternative channel materials to Si for next generation metal–oxide–semiconductor field-effect transistors (MOSFETs) [1]. Recent research in photonics has demonstrated direct-bandgap Ge and SiGe by realizing these materials in their hexagonal lattice structure [2, 3]. The potential compatibility of these materials with Si electronics makes nanoleds and nanolasers of hexagonal Ge and SiGe attractive options for monolithic optoelectronic integrated circuits. The relatively small bandgap of Ge makes this material also a favorable choice as bottom sub-cell in multi-junction space solar cells [4, 5].

The potential of Ge in these applications is hampered by a high density of electronic defects at its surface. In MOSFETs, these defects can lower the sub-threshold slope [6–8] and lead to a compromised carrier channel mobility [9, 10], while in nanolasers [11–13] and solar cells [14, 15] these defects can act as non-radiative recombination centers for electrons and holes which decrease the conversion efficiency. Surface

passivation of Ge is essential to mitigate these effects. Atomic layer deposition (ALD) is a deposition technique that allows the preparation of ultrathin films that can passivate the surface of nanolaser cavities and solar cell's absorber layers. In MOSFETs dielectric films can passivate the top surface of the channel and simultaneously act as gate-oxide. ALD is especially suited for these purposes since it enables sub-nanometer thickness control combined with excellent conformality on high aspect ratio structures.

Most research on ALD films for surface passivation is conducted in the context of Si photovoltaics. These studies have demonstrated that ALD Al₂O₃ on Si provides excellent passivation [15–17]. The nature of this surface passivation is twofold. First, ALD of Al₂O₃ on Si leads to the formation of an ultrathin (~1.5 nm) high-quality silicon oxide (SiO_x) layer between Si and Al₂O₃ [16]. The remaining defects at this Si/SiO_x interface are predominantly silicon dangling bonds (Pb-type defects) [15, 18], which are effectively passivated by atomic hydrogen [19–21] provided to and/or kept at this Si/SiO_x interface by the Al₂O₃ passivation layer during a post-deposition anneal (PDA) [22]. This mechanism leads to an interface defect density (D_{it}) as low as $D_{it} \leq 1 \times 10^{11} \text{ cm}^{-2} \text{ eV}^{-1}$

[15]. Secondly, Al_2O_3 yields a high negative fixed charge density (Q_f) when deposited on Si ($Q_f = 4\text{--}13 \times 10^{12} \text{ cm}^{-2}$) [15]. This fixed charge forms an electrical field that leads to a space charge region in the silicon and hence enhanced surface passivation [23]. This mechanism is referred to as field-effect passivation. The combination of a low D_{it} and a high Q_f leads to a low surface recombination velocity (S_{eff}), a common metric of surface losses in solar cells and nanolasers. For Si/ Al_2O_3 , surface recombination velocities can be as low as $S_{eff} \leq 10 \text{ cm s}^{-1}$ [16, 24, 25].

ALD Al_2O_3 is a known passivation layer for germanium (Ge) where it is mainly explored for application in MOSFETs [9, 26–30]. ALD of Al_2O_3 as passivation layer on Ge has been shown to lead to the formation of a germanium oxide (GeO_x) interlayer [27, 31, 32], somewhat similar to the SiO_x interlayer formed by ALD Al_2O_3 on Si. It is, however, debated whether such an interfacial GeO_x layer is beneficial or not. In contrast to SiO_2 , GeO_2 is traditionally regarded as undesired due to its limited thermal stability [9, 33–35] and water solubility [9, 36]. Yet recent DFT calculations [30, 37] and several experimental studies have shown that a Ge/ GeO_2 interface with a low defect density is possible ($D_{it} \leq 10^{11} \text{ cm}^{-2} \text{ eV}^{-1}$) [38–40]. Most research with respect to ALD Al_2O_3 on Ge was therefore aimed at understanding and engineering the GeO_x layer between Ge and Al_2O_3 [29–31, 39, 41–43]. It has been reported that D_{it} can be lowered by a factor 10 to 100 by addressing this interlayer [26, 29, 30]. Especially plasma post-oxidation of the Ge/ Al_2O_3 stack has proven successful ($D_{it} \leq 10^{11} \text{ cm}^{-2} \text{ eV}^{-1}$) [26]. Research regarding the ALD Al_2O_3 process parameters themselves has remained very limited. Such parameters include the Al_2O_3 film thickness, substrate temperature, and post-deposition anneal. This is remarkable since these parameters have proven to be very important for the passivation of Si by ALD Al_2O_3 [25, 44]. Also, the role of field-effect passivation in the Ge/ Al_2O_3 system appears to be unexplored and reports on the surface recombination velocity of this interface are rare.

In this work, we have systematically investigated the effect of the ALD Al_2O_3 process parameters on the surface passivation of Ge. The passivation quality is determined using the upper limit of the surface recombination velocity $S_{eff,max}$, which means that the crude assumption is made that the Ge bulk lifetime is infinite, i.e., not limiting. The process parameters investigated include the Al_2O_3 film thickness (1–44 nm), deposition temperature (50–350 °C), and post-deposition anneal temperature (300–600 °C). For the synthesis of the Al_2O_3 films, we used a plasma-enhanced ALD process since it allows for a lot of freedom in processing conditions [45]. Additionally, we monitored the temporal stability of the Ge surface passivation and determined the magnitude of the fixed charge density of Al_2O_3 to shed light on the role of field-effect passivation. To better

understand our results, we utilized the very extensive knowledge about the Al_2O_3 passivation of Si. We did this by making a 1-to-1 comparison with the surface passivation of Si by ALD Al_2O_3 using earlier results from our research group that were obtained using the same methodologies and experimental tools as for the Ge surface passivation.

Results

Influence of Al_2O_3 thickness, substrate temperature, and annealing temperature on S_{eff}

The surface recombination velocity for germanium at room temperature has been investigated as a function of the Al_2O_3 film thickness, ALD substrate temperature, post-deposition annealing temperature, and storage time. The results are shown in Figs. 1, 2, 3 and 4. In Fig. 1, the surface recombination velocity is displayed for Al_2O_3 films up to 44 nm thick. The figure shows the surface recombination velocity right after the post-deposition anneal and 3 months later. Right after annealing, two trends seem to be present: an increasing trend of $S_{eff,max}$ for Al_2O_3 thicknesses up to 6 nm and a decreasing trend for Al_2O_3 thicknesses > 6 nm. The two trends seem to behave differently upon aging. For $\text{Al}_2\text{O}_3 > 6 \text{ nm}$, aging results in a similar decrease of $S_{eff,max}$. Below 6 nm we observed only a slight improvement for the 1 nm Al_2O_3 film and no change for the 3 nm film upon annealing. Note that since the 3 nm sample deviates from the trend, we repeated the experiment with an independently prepared sample. This gave the same result indicating that the local maximum in $S_{eff,max}$ at 3 nm after aging is not an artifact. With regard to the magnitude of the surface recombination we find a minimum of $S_{eff,max} \approx 200 \text{ cm s}^{-1}$ for a film thickness of 44 nm and a maximum of $S_{eff,max} \approx 1800 \text{ cm s}^{-1}$ for 3 nm Al_2O_3 . These observations for Ge are distinct from those of Si, where a monotonically decreasing trend for $S_{eff,max}$ is observed [41, 46] and surface recombination velocities drop to values as low as $S_{eff,max} \leq 10 \text{ cm s}^{-1}$ for thicknesses above 10 nm [16, 24, 25].

The impact of the germanium substrate temperature during ALD on the passivation quality is shown in Fig. 2. Films deposited at lower substrate temperatures seem to passivate the germanium surface better ($S_{eff,max} \approx 170 \text{ cm s}^{-1}$). The value of $S_{eff,max}$ increases up to 350 °C. This is in contrast with the case of Si, where an optimum was found at $T_{sub} = 150\text{--}200 \text{ °C}$.

In Fig. 3 the effect of the post-deposition annealing temperature on the passivation quality is presented. In the as-deposited state, a very high surface recombination velocity was found ($S_{eff,max} \approx 1.8 \times 10^4 \text{ cm s}^{-1}$); i.e., the Al_2O_3 films provide hardly any passivation. Annealing of the wafers yielded a substantial reduction in $S_{eff,max}$. The optimal anneal temperature

was found to be around 425 °C, at which $S_{\text{eff,max}}$ was reduced to $S_{\text{eff,max}} \approx 1.0 \times 10^3 \text{ cm s}^{-1}$. Substantial improvements in surface passivation around this annealing temperature were also found by others investigating Ge/ Al_2O_3 stacks [9, 27, 38]. Interestingly, the optimum for germanium coincides with the optimum anneal temperature of 400–450 °C for Si [25].

Besides annealing, aging of the Al_2O_3 passivated wafers showed remarkable improvements in surface passivation as seen in Figs. 1 and 2. In Fig. 4 we report on this improvement by plotting $S_{\text{eff,max}}$ versus the number of storage days after the PDA. For this experiment, a wafer with 22 nm Al_2O_3 was stored in the dark at room temperature. In the first 30 days the surface recombination velocity drops from $S_{\text{eff,max}} \approx 1770 \text{ cm s}^{-1}$ to $S_{\text{eff,max}} \approx 270 \text{ cm s}^{-1}$. After 30 days, the surface recombination velocity stabilizes. In some cases, such an effect has also been observed to a limited extent for Si wafers passivated with Al_2O_3 [47].

Determination of fixed charge density

In the previous section, we showed the effect of various process parameters on the surface recombination velocity. In this section we discuss the fixed charge density of the Ge/ Al_2O_3 stack, as determined by corona charging experiments. In Fig. 5 the surface recombination velocity is plotted versus the deposited corona charge Q_c for Ge passivated with 22 nm Al_2O_3 deposited at substrate temperature $T_{\text{Sub}} = 200 \text{ °C}$ and annealed at 425 °C for 10 min in N_2 ambient. First $S_{\text{eff,max}}$ increases and

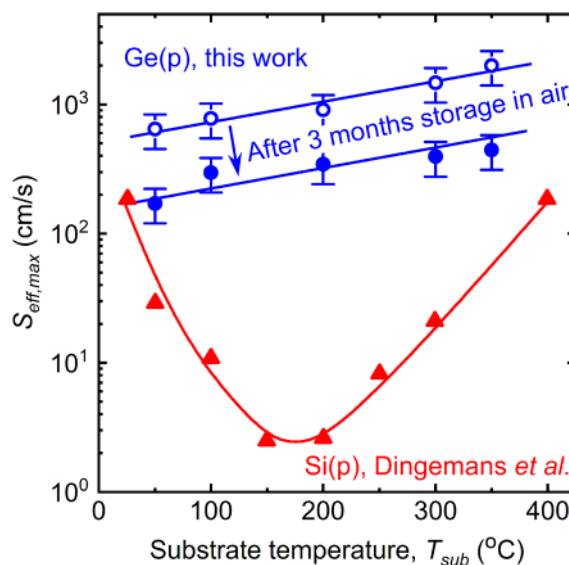


Figure 2: Effective surface recombination velocity $S_{\text{eff,max}}$ as a function of the substrate temperature used during the deposition of Al_2O_3 films on Ge and Si. The in this graph corresponds to 22 nm Al_2O_3 on $\sim 0.3 \text{ } \Omega \text{ cm}$ (100) p-type germanium annealed at 425 °C for 10 min in N_2 ambient (this work) and 30 nm Al_2O_3 on $\sim 2 \text{ } \Omega \text{ cm}$ p-type silicon annealed at 400 °C for 10 min in N_2 ambient (data from Dingemans et al. [24]). The Ge samples were stored in air at room temperature.

subsequently it decreases. A maximum in $S_{\text{eff,max}}$ is reached for a positive corona charge density of $(1.8 \pm 0.5) \times 10^{12} \text{ cm}^{-2}$. This means that the fixed charge density of the Al_2O_3 is

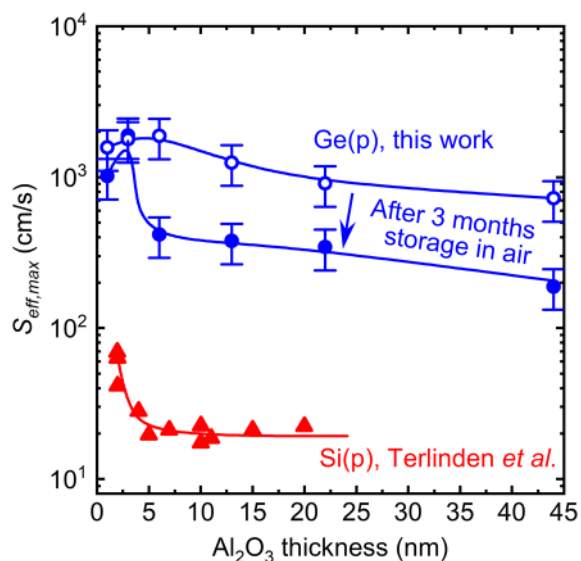


Figure 1: Effective surface recombination velocity $S_{\text{eff,max}}$ measured on Ge ($\sim 0.3 \text{ } \Omega \text{ cm}$ p-type, (100)) and Si ($\sim 1.5 \text{ } \Omega \text{ cm}$ p-type) as a function of the plasma-enhanced ALD Al_2O_3 film thickness using a substrate temperature of 200 °C and a post-deposition annealing treatment at 425 °C for 10 min in N_2 ambient. The samples were stored in air at room temperature. The data for Si have been taken from Terlinden et al. [41].

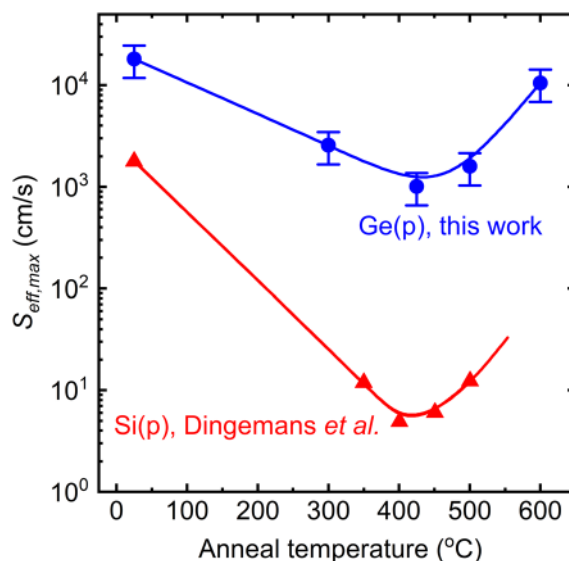


Figure 3: Effective surface recombination velocity $S_{\text{eff,max}}$ as a function of the post-deposition anneal temperature (N_2 ambient). A single sample was annealed in consecutive steps of 10 min. The anneal temperature '25 °C' refers to the as-deposited state; i.e., without anneal. The wafers concern germanium ($\sim 400 \text{ } \mu\text{m}$, $\sim 0.3 \text{ } \Omega \text{ cm}$, p-type, (100)) and silicon ($\sim 275 \text{ } \mu\text{m}$, $\sim 2.2 \text{ } \Omega \text{ cm}$, p-type, (100)) covered with, respectively, 22 nm and 30 nm Al_2O_3 . The data concern measurements performed directly after PDA. The data for Si have been taken from Dingemans et al. [25].

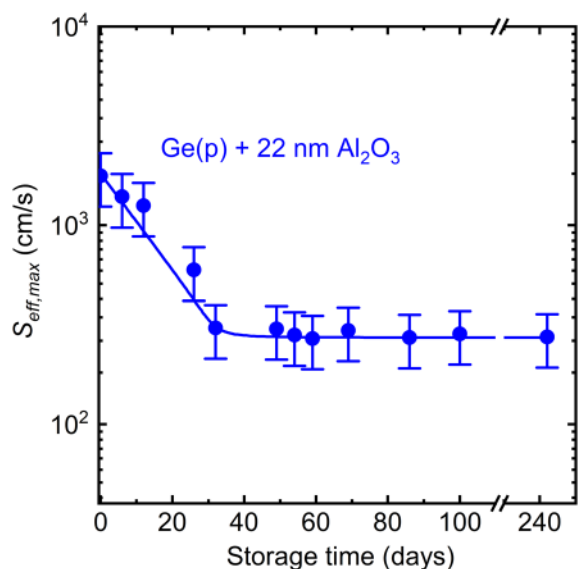


Figure 4: Surface recombination velocity of a single germanium wafer ($\sim 0.3 \Omega \text{ cm}$, p-type, (100)) passivated with 22 nm plasma-enhanced ALD Al_2O_3 film as a function of storage time in air at room temperature. The Al_2O_3 film has been deposited at 200°C and annealed at 425°C for 10 min in N_2 ambient.

negative with magnitude $Q_f = (1.8 \pm 0.5) \times 10^{12} \text{ cm}^{-2}$. This fixed charge can arise from the $\text{GeO}_x/\text{Al}_2\text{O}_3$ interface and/or Al_2O_3 bulk. Measurements of the 5 nm and 44 nm thick Al_2O_3 films revealed only a mild increase in Q_f with increasing film thickness.

The maximum $S_{\text{eff,max}}$ in Fig. 5 is related to the D_{it} and indicates the level of chemical passivation [49]. For Ge this value is about 8 times larger than for Si ($S_{\text{eff,max}} \approx 117 \text{ cm s}^{-1}$), which implies a substantial difference in the chemical passivation. Note that for Ge a double peak appears to be present in Fig. 5. Such a feature can arise due to several reasons including the presence of two distinct defect states and slight asymmetry of the wafer surfaces (note that 2 separate ALD runs are required to cover both sides of the wafer).

Presence of interfacial oxide

We investigated the interfacial oxide by using a combination of XPS and cross-sectional TEM. XPS was performed on Ge substrates covered with 4 nm Al_2O_3 . Figure 6a displays the spectra of the Ge 3d peak for Ge covered with Al_2O_3 deposited at 200°C before and after annealing at 425°C for 10 min. In these spectra, two distinct peaks arise. The first peak arises at a binding energy of about 30 eV which corresponds to Ge–Ge bonds from the Ge substrate. The second peak arises at about 32.8 eV and corresponds to Ge–O bonds. The presence of this peak indicates that a GeO_x interlayer exists between the Ge substrate and the 4 nm Al_2O_3 . This interlayer is already present before annealing, which means that the GeO_x forms during the ALD process itself.

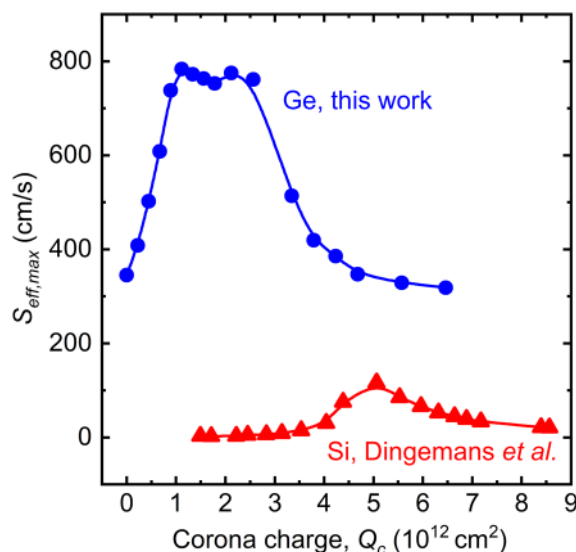


Figure 5: Effective surface recombination velocity S_{eff} as a function of the deposited corona charge density. The data for germanium are obtained for germanium passivated with a 22 nm plasma-enhanced ALD Al_2O_3 film deposited at 200°C and annealed at 425°C for 10 min. The data for silicon have been taken from Dingemans et al. [24] and represent a 30 nm plasma-enhanced ALD Al_2O_3 film deposited at 200°C and annealed at 400°C for 10 min.

The subsequent annealing did not induce notable changes in the interlayer as observable by XPS. Figure 6b shows the spectra of the Ge 3d peak for annealed Al_2O_3 deposited at various temperatures ($50\text{--}350^\circ\text{C}$). For all conditions a clear peak around 32.8 eV is observed, which discloses that a GeO_x interlayer is formed. The area of such a peak relates to the amount of detected Ge–O bonds, while the peak position is associated with the stoichiometry of the GeO_x (i.e., the oxidation state of Ge). The area of the GeO_x peak increases with deposition temperature suggesting the growth of a thicker interlayer at elevated deposition temperatures. The Ge 3d peak position at 32.8 eV remains virtually the same which implies no major differences in stoichiometry of the GeO_x .

A cross-sectional TEM image of a Ge/ Al_2O_3 stack is shown in Fig. 7a along with the earlier results on Si (Fig. 7b). For the case of Si, we observed a clear SiO_x interlayer, which is about 1.5 nm thick. The TEM on Ge yielded unfortunately no clear image of the interlayer due to a low contrast between the GeO_x and Al_2O_3 [48]. Yet, from integrated image brightness contrast profiles across the layer stack, acquired both using bright-field TEM as well as high-angle annular dark field STEM, we estimate the GeO_x interlayer to be $2.2 \pm 0.3 \text{ nm}$ thick. A confirmation of the layer thickness using an EDX elemental profile was not successful due to the sensitivity of the Al_2O_3 layer for the electron beam. On the other hand, the beam sensitivity of the Al_2O_3 layer

only created a contrast between the two oxide layers, again yielding a GeO_x layer thickness of ~ 2.3 nm.

Discussion

In this work, we have presented the role of several process parameters on the surface passivation of Ge by ALD Al_2O_3 together with the determination of the fixed charge density and temporal stability of the passivation.

In the introduction, we mentioned that post-oxidation techniques of the $\text{Ge}/\text{GeO}_x/\text{Al}_2\text{O}_3$ stacks have proven to be very beneficial for the surface passivation of Ge. The parameter study performed in this work shows various process aspects of the $\text{Ge}/\text{GeO}_x/\text{Al}_2\text{O}_3$ stack (anneal temperature, film thickness, etc.) yield comparable effects on the surface passivation. The post-deposition anneal treatment was found to have the strongest effect on the surface passivation. The latter showed an improvement by a factor 18 for $S_{\text{eff,max}}$ reached after an optimum PDA (10 min at 400 °C) and no PDA. Film thickness showed an important effect as well, since an increase of the Al_2O_3 film from 1 to 44 nm lowered $S_{\text{eff,max}}$ by a factor 8. Aging of the $\text{Ge}/\text{GeO}_x/\text{Al}_2\text{O}_3$ stack for 30 days resulted in a similar improvement (about a factor of 6.5). Lastly, we found that the deposition temperature has only a relatively mild influence on the surface passivation: decreasing the deposition temperature from 350 to 50 °C results in an improvement of $S_{\text{eff,max}}$ by only a factor of 2.5. The importance of these findings is that they enlarge the possibilities to fabricate well passivated $\text{Ge}/\text{GeO}_x/\text{Al}_2\text{O}_3$ interfaces which can improve the performance of Ge-based (opto)electronic devices.

The peak heights of $S_{\text{eff,max}}$ in Fig. 5 are proportional to the level of chemical passivation [49]. For the Ge surface passivated by Al_2O_3 this $S_{\text{eff,max}}$ peak is substantially higher than for the Si surface passivated by Al_2O_3 , indicating a lower level of chemical passivation of the former. This finding is in accordance with literature where interface defect densities for $\text{Si}/\text{Al}_2\text{O}_3$ are commonly reported around $D_{\text{it}} \sim 1 \times 10^{11} \text{ cm}^{-2} \text{ eV}^{-1}$ [15], while for $\text{Ge}/\text{Al}_2\text{O}_3$ values are reported between $D_{\text{it}} = 5 \times 10^{11} \text{ cm}^{-2} \text{ eV}^{-1}$ and $1 \times 10^{13} \text{ cm}^{-2} \text{ eV}^{-1}$ [10, 26, 27, 42] (at least without intentionally increasing the thickness of the GeO_x interlayer by for example an additional post-oxidation plasma step [26], see also introduction). A different nature of the interface defects involved could lay at the heart of this difference between Si and Ge. For the Si/SiO_2 interface, it is well known that stretched Si bonds and Si dangling bonds [43, 50–52] form the dominant defects. For the Ge/GeO_x interface, there seems less consensus. Various possibilities are proposed including: Ge–M bonds (with $M = \text{Hf}, \text{Zr}, \text{etc.}$) [53], sub-stoichiometric GeO_x [30], and Ge-dangling bonds [37, 54]. Especially the latter is topic of debate [37, 54–58], which indicates a key difference between the $\text{Ge}/\text{GeO}_x/\text{Al}_2\text{O}_3$ and the $\text{Si}/\text{SiO}_x/\text{Al}_2\text{O}_3$ interface. Also, the role of hydrogen as passivating agent for Ge-dangling bonds appears controversial [55–58].

In the debate about Ge-dangling bonds, an extensive study by Stesmans et al. [58] concluded that Ge-dangling bonds at the Ge surface can be passivated by hydrogen, but only partially ($\sim 60\%$ max). Assuming a less prominent role of hydrogen in the chemical passivation of the Ge/GeO_x interface, the differences between Si and Ge in the dependence of $S_{\text{eff,max}}$ upon Al_2O_3

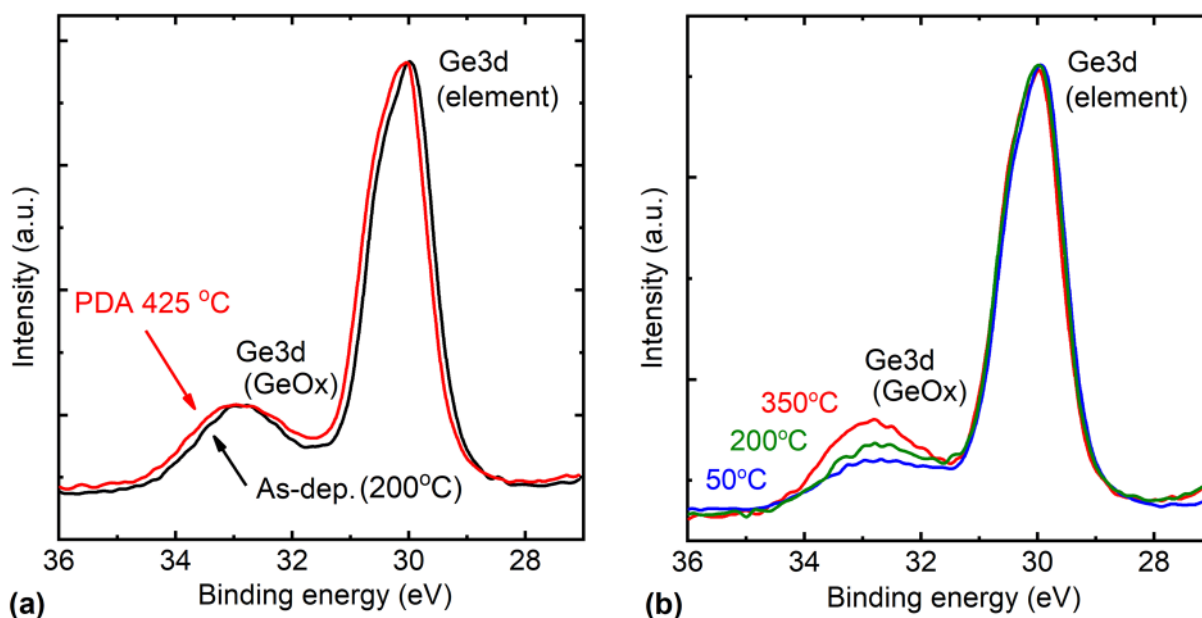


Figure 6: XPS spectra of the germanium Ge 3d peak. The measurements were performed on a Ge substrate passivated with 4 nm Al_2O_3 prepared by plasma-enhanced ALD. (a) Scans for a film deposited at 200 °C before and after a 10 min PDA at 425 °C. (b) Scans for films deposited at 50 °C, 200 °C, and 350 °C after annealing for 10 min at 425 °C.

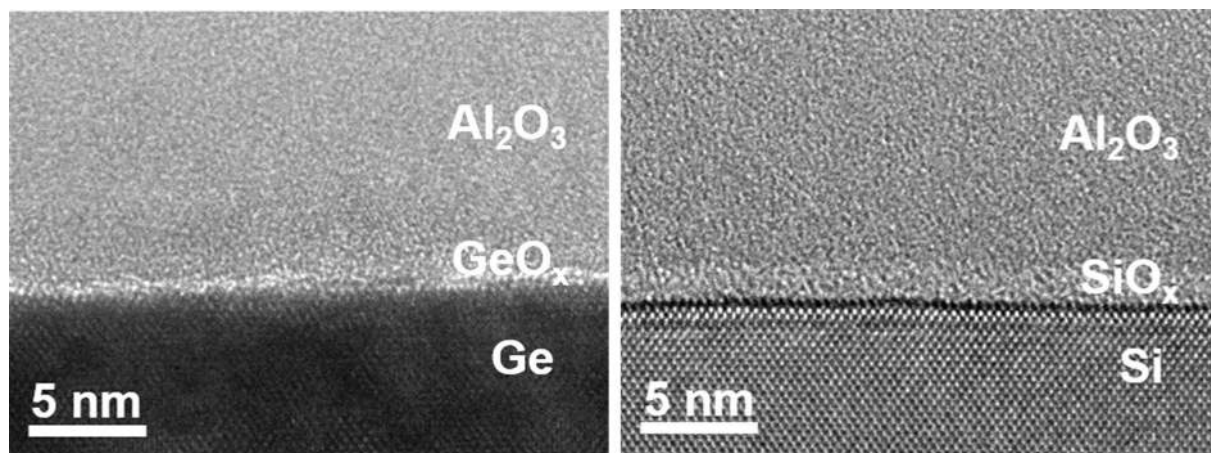


Figure 7: (a) Cross-sectional bright-field transmission electron microscopy image of the interface between p-type germanium and 20 nm plasma-enhanced ALD Al_2O_3 synthesized at 200 °C and annealed at 425 °C for 10 min in N_2 ambient. The sample has been prepared by FIB. (b) Transmission electron microscopy (TEM) cross-sectional image of the interface between p-type silicon and 20 nm plasma-enhanced ALD Al_2O_3 synthesized at 200 °C and annealed at 425 °C for 30 min in N_2 ambient. The interface is characterized by a 1.5 nm thick SiO_x interlayer. The sample has been prepared by tripod polishing. Figure is adapted from Hoex et al. [16].

substrate temperature as observed in Fig. 2 may not be so surprising. The effectiveness of the Si dangling bonds hydrogenation process during annealing depends on a complex interplay between the Al_2O_3 microstructure and the hydrogen content of the film, which both vary with substrate temperature [22]. At lower substrate temperatures (below 200 °C) [22] a fairly high hydrogen content is obtained, while higher substrate temperatures (especially above 200 °C) [22] result in denser films which effuse less hydrogen during annealing. The trade-off between these properties leads to an optimum substrate temperature of $T_{\text{sub}} \approx 200$ °C [22]. If this hydrogenation process is indeed less effective for passivation of remaining defects at the Ge/GeO_x interface, it can be understood that the dependence on substrate temperature may be very different.

The post-deposition annealing temperature results indicate an optimum annealing temperature around 425 °C (Fig. 3) which is similar to the optimum annealing temperature for Si [44]. The knowledge that for Si optimal hydrogenation occurs around 400 °C, and that the activation energies for the hydrogenation reactions of Ge and Si dangling bonds are similar (1.44 eV and 1.51 eV respectively [58]), seem to favor the argument for hydrogenation as a passivation mechanism for Ge. The role of hydrogenation seems, however, less than for Si, because Fig. 3 shows that the improvement of $S_{\text{eff,max}}$ with this optimum annealing treatment is substantially less for Ge/ Al_2O_3 than for Si/ Al_2O_3 . These two conclusions resonate with the results of Stesmans et al. [58] who states that: hydrogenation passivates only a certain fraction of the Ge-dangling bonds and that this process is optimal around 375 °C.

The origin of the positive effect of aging on $S_{\text{eff,max}}$ is not yet understood (Fig. 4). Multiple possibilities exist. A first reason could be filling of oxide traps at the GeO_x/ Al_2O_3 interface

which contribute to a higher Q_f . For Si/ Al_2O_3 this was observed when exposed to ultraviolet light for prolonged time [47]. Our samples, however, were stored in the dark. Alternatively, the O_2 plasma in the ALD process could have induced interface and/or bulk defects by the energetic photons it emits [59]. Post-deposition curing of these defects might cause $S_{\text{eff,max}}$ to decrease over time. This process may already occur during annealing but can continue to proceed at a slower pace during storage at room temperature.

For Si/ $\text{SiO}_x/\text{Al}_2\text{O}_3$, the fixed charge density is reported to be virtually constant with Al_2O_3 film thickness [41]. The measured values for plasma-enhanced ALD Al_2O_3 range from $Q_f = 4 \times 10^{12} \text{ cm}^{-2}$ to about $Q_f = 13 \times 10^{12} \text{ cm}^{-2}$ [23, 24, 60, 61]. We determined the fixed charge density to be $Q_f = -(1.8 \pm 0.5) \times 10^{12} \text{ cm}^{-2}$ (Fig. 5). As for Si, the nature of the charge is found to be negative. Moreover, we observed only a mild increase in Q_f with film thickness, which indicates that most of this charge resides near the interface with Ge. A difference with Si is the magnitude of Q_f , which is found to be lower. The significance of these findings is that they shed light on the field-effect passivation of Ge induced by Al_2O_3 . This field-effect passivation is most relevant for devices like nanolaser and solar cells. Due to the electron-repelling effect of the negative fixed charge in the Al_2O_3 , the induced field-effect passivation works more effectively on p-type doped Ge.

A GeO_x interlayer was found to consistently form during the ALD process (Fig. 6a, b). The oxygen plasma used in our ALD process can contribute to its formation. We found by XPS that the interlayer grows thicker for higher substrate temperatures (Fig. 6b), an effect that can be attributed to enhanced diffusion of the oxygen species through the GeO_x. In contrast to some earlier reports [27, 29, 62], this increasing GeO_x interlayer with

substrate temperature did not result in better surface passivation (Fig. 2).

Conclusion

In this study, we elucidated the effect of the Al_2O_3 film thickness, deposition temperature and anneal temperature on the surface passivation of Ge by ALD Al_2O_3 . It has been found that optimization of these process parameters can enable a reduction of $S_{\text{eff,max}}$ up to an order of magnitude, resulting in surface recombination velocities as low as $S_{\text{eff,max}} = 170 \text{ cm s}^{-1}$. This information provides guidance for designing well passivated Ge/ GeO_x / Al_2O_3 interfaces. We also determined the fixed charge density of the Ge/ GeO_x / Al_2O_3 stack to be $Q_f = -(1.8 \pm 0.5) \times 10^{12} \text{ cm}^{-2}$. This value implies that $S_{\text{eff,max}}$ benefits from a certain degree of field-effect passivation, which can be especially beneficial for p-type Ge surfaces. Finally we found that the passivation quality improves during storage in air after which it finally becomes stable.

Experimental details

For the experiments, we used double side polished p-type Ge wafers ($\sim 400 \mu\text{m}$, $\langle 100 \rangle$, $\rho = 0.2\text{--}0.4 \Omega \text{ cm}$, dopant: gallium) procured from Umicore. The native oxide was removed from the germanium substrates by dipping in diluted hydrofluoric acid (1%, 90 s) followed by deionized water rinsing (90 s) and N_2 blow-drying. The wafers were coated on both sides with ALD Al_2O_3 in a FlexAL™ system from Oxford Instruments, which is described in detail elsewhere [63]. The first half cycle consists of vapor drawn dosing the Al-precursor trimethylaluminum [TMA, $\text{Al}(\text{CH}_3)_3$, 99.999% pure, Dockweiler Chemicals]. A remote oxygen plasma is used as co-reactant in the second half cycle of the ALD process. The substrate temperature was kept constant during the deposition runs at a chosen value between 50 and 350 °C. At the start of each deposition, the wafers were subjected to a warmup step of 10 min in N_2 ambient. After deposition, the wafers received a post-deposition anneal (PDA) to activate the passivation [25]. The annealing was performed for 10 min in N_2 ambient (N_2 gas purity > 99.999%) at 425 °C using a Jipelec Rapid Thermal Annealer unless stated differently. The thickness of the ALD Al_2O_3 films was measured by spectroscopic ellipsometry using a J.A. Woollam Co., Inc. M2000 rotating compensator spectroscopic ellipsometer.

To measure the effective excess carrier lifetime [τ_{eff} (s)] in Al_2O_3 passivated Ge wafers, we used the commercially available WCT-120 Photoconductance Lifetime Tester. This tool is well known in the research field of silicon solar cells and was originally developed to measure carrier lifetime in silicon wafers. The technique is referred to as quasi-steady-state photoconductance (QSSPC) and its operating principle can be found in the work

of Cuevas and colleagues [64]. To make the tool suitable for Ge wafers we followed a similar approach as proposed by Cornagliotti et al. [65]. From the effective excess carrier lifetime one can derive an upper limit of the surface recombination velocity [$S_{\text{eff,max}}$ (cm s^{-1})] by assuming that the bulk of the wafer has a negligible effect on τ_{eff} compared to the surface; i.e., the bulk lifetime is assumed to be infinite. The maximum surface recombination velocity is a well-established metric to express the surface passivation [66]:

$$S_{\text{eff,max}}(\Delta n) \approx \frac{W}{2\tau_{\text{eff}}(\Delta n)}, \quad (1)$$

where Δn (cm^{-3}) is the average excess carrier density in the wafer and W (cm) is the wafer thickness. For this expression we thus assume that τ_{eff} is surface limited and that $S_{\text{eff,max}}$ is not diffusion limited. We report $S_{\text{eff,max}}$ for $\Delta n = 10^{15} \text{ cm}^{-3}$, the standard for Si. The measurement uncertainty in $S_{\text{eff,max}}$ is determined from the uncertainties in the parameters used to calculate the lifetime and surface recombination velocity from the measured quantities of the WCT-120 Photoconductance Lifetime Tester.

The stability of the Ge passivation was monitored over the course of 240 days by regularly performing QSSPC measurements. The wafers were stored in the dark under ambient conditions.

Surface passivation can be established by two different mechanisms [23]. The first is a reduction of the interface defect density (D_{it}) at the semiconductor surface. This mechanism is commonly referred to as chemical passivation. The second mechanism is a significant reduction of either the electron or hole concentration at the surface. This can be achieved by an electric field which can be induced by fixed charge (Q_f) in the dielectric film deposited on the semiconductor surface. This type of passivation is referred to as field-effect passivation. To determine the contribution of field-effect passivation to the passivation of the Ge surface by Al_2O_3 we conducted corona charge experiments [67–69]. For this purpose, incremental positive or negative charge was deposited on the surface of the passivated Ge wafer using ionized air molecules created by a needle with a DC voltage of $\pm 10 \text{ kV}$ with respect to the sample using the Corona Charging System of Delft Spectral Technologies. After each corona charge step, both the $S_{\text{eff,max}}$ and the deposited surface charge density were measured. The former was obtained with the QSSPC method and the latter with Kelvin probe potential measurements that were conducted in the Corona Charging System. Repetition of these steps allowed us to plot the deposited corona charge (Q_c) versus $S_{\text{eff,max}}$. The point of maximum $S_{\text{eff,max}}$ provides the fixed charge density. At this point applies: $Q_f = -Q_c$.

X-ray photoelectron spectroscopy (XPS) provided information about the chemical composition of the films and the Ge– Al_2O_3 interface. A Thermo Scientific KA1066 spectrometer

employing monochromatic Al K α ($h\nu = 1486.6$ eV) X-rays radiation was used. The background subtraction method for the XPS data was a Shirley background with the additional constraint that the background should not be of greater intensity than the actual data at any point in the region. The adventitious carbon C–C peak at 284.8 eV was used as charge correction reference. The transmission electron microscopy (TEM) study was performed using a probe-corrected JEOL ARM operated at 200 kV and equipped with a 100 mm² Centurio SDD energy dispersive X-ray spectroscopy (EDS) detector. Cross-sectional TEM samples were made using a standard lift-out focused ion beam (FIB) preparation protocol [70].

Acknowledgments

This work was supported by the Gravitation Program “Research Centre for Integrated Nanophotonics” (Grant Number 024.002.033) of The Netherlands Organization for Scientific Research (NWO). The work of J. Melskens and B. Macco was supported by The Netherlands Organization for Scientific Research under the Dutch TTW-VENI Grants 15896 and 16775, respectively. The authors acknowledge Cristian van Helvoirt, Barathi Krishnamoorthy, Patrick Bax and Martijn Dijkstra for their technical assistance. B. Barcones is acknowledged for the Focused Ion Beam preparation of the TEM sample. Solliance and the Dutch Province of Noord Brabant are acknowledged for funding the TEM Facility. We are furthermore grateful for the germanium wafers and support provided by Umicore.

Open access

This article is licensed under a Creative Commons Attribution 4.0 International License, which permits use, sharing, adaptation, distribution and reproduction in any medium or format, as long as you give appropriate credit to the original author(s) and the source, provide a link to the Creative Commons licence, and indicate if changes were made. The images or other third party material in this article are included in the article's Creative Commons licence, unless indicated otherwise in a credit line to the material. If material is not included in the article's Creative Commons licence and your intended use is not permitted by statutory regulation or exceeds the permitted use, you will need to obtain permission directly from the copyright holder. To view a copy of this licence, visit <http://creativecommons.org/licenses/by/4.0/>.

References

1. P.S. Goley, M.K. Hudait, Germanium based field-effect transistors: challenges and opportunities. *Materials* 7(3), 2301–2339 (2014)

2. H.I.T. Hauge, S. Conesa-Boj, M.A. Verheijen, S. Koelling, E.P.A.M. Bakkers, Single-crystalline hexagonal silicon–germanium. *Nano Lett.* 17(1), 85 (2017)
3. E.M.T. Fadaly, A. Dijkstra, J.R. Suckert, D. Ziss, M.A.J. Van Tilburg, C. Mao, Y. Ren, V.T. Van Lange, K. Korzun, S. Kölling, M.A. Verheijen, D. Busse, C. Rödl, J. Furthmüller, F. Bechstedt, J. Stangl, J.J. Finley, S. Botti, J.E.M. Haverkort, E.P.A.M. Bakkers, Direct-bandgap emission from hexagonal Ge and SiGe alloys. *Nature* 580, 205 (2020)
4. C. Weiss, J. Schön, O. Höhn, C. Mohr, R. Kurstjens, B. Boizot, S. Janz, S. Irradiés, Potential analysis of a rear-side passivation for multi-junction space solar cells based on germanium substrates. In *2018 IEEE 7th World Conference on Photovoltaic Energy Conversion*, Waikoloa Village, Hawaii, United States, 2018, pp. 3392–3396
5. S. Janz, C. Weiss, R. Kurstjens, B. Boizot, B. Fuhrmann, V. Khorenko, S. Irradiés, Amorphous silicon carbide rear-side passivation and reflector layer stacks for multi-junction space solar cells based on germanium substrates. In *2017 IEEE 44th Photovoltaic Specialist Conference*, Washington, DC, United States, 2017, pp. 83–87
6. S.M. Sze, K.K. Ng, *Physics of Semiconductor Devices*, 3rd edn. (Wiley, Hoboken, 2007).
7. C. Dou, A Study on Interface Traps and Near Interfacial Bulk Traps at the Interfaces of Dielectric Semiconductor and Semiconductor Heterojunction, Doctoral Dissertation, Tokyo Institute of Technology, 2014
8. M. Hauck, J. Lehmeier, G. Pobegen, H.B. Weber, M. Krieger, An adapted method for analyzing 4H silicon carbide metal–oxide–semiconductor field-effect transistors. *Commun. Phys.* (2019). <https://doi.org/10.1038/s42005-018-0102-8>
9. Q. Xie, S. Deng, M. Schaekers, D. Lin, M. Caymax, A. Delabie, X.P. Qu, Y.L. Jiang, D. Deduytsche, C. Detavernier, Germanium surface passivation and atomic layer deposition of high-k dielectrics—a tutorial review on Ge-based MOS capacitors. *Semicond. Sci. Technol.* 27(7), 1–12 (2012)
10. J. Sun, J. Lu, Interface engineering and gate dielectric engineering for high performance Ge MOSFETs. *Adv. Condens. Matter Phys.* 2015, 1–9 (2015)
11. A. Higuera-Rodriguez, B. Romeira, S. Birindelli, L.E. Black, E. Smalbrugge, P.J. Van Veldhoven, W.M.M. Kessels, M.K. Smit, A. Fiore, Ultralow surface recombination velocity in passivated InGaAs/InP nanopillars. *Nano Lett.* 17(4), 2627 (2017)
12. K. Ding, C.Z. Ning, Metallic subwavelength-cavity semiconductor nanolasers. *Light Sci. Appl.* 1(7), 1 (2012)
13. M.T. Hill, M.C. Gather, Advances in small lasers. *Nat. Photonics* 8(12), 908 (2014)
14. J. Melskens, B.W.H. Van De Loo, B. Macco, L.E. Black, S. Smit, W.M.M.E. Kessels, Passivating contacts for crystalline silicon solar cells : from concepts and materials to prospects. *IEEE J. Photovolt.* 8(2), 373 (2018)

15. G. Dingemans, W.M.M. Kessels, Status and prospects of Al₂O₃-based surface passivation schemes for silicon solar cells. *J. Vac. Sci. Technol. A* **30**(4), 1–24 (2012)
16. B. Hoex, S.B.S. Heil, E. Langereis, M.C.M. Van De Sanden, W.M.M. Kessels, Ultralow surface recombination of c-Si substrates passivated by plasma-assisted atomic layer deposited Al₂O₃. *Appl. Phys. Lett.* **89**(4), 9 (2006)
17. B. Liao, B. Hoex, A.G. Aberle, D. Chi, C.S. Bhatia, Excellent c-Si surface passivation by low-temperature atomic layer deposited titanium oxide. *Appl. Phys. Lett.* **104**(25), 3 (2014)
18. A. Stesmans, V.V. Afanas'ev, Paramagnetic defects in annealed ultrathin layers of SiO_x, Al₂O₃ and ZrO₂ on (100)Si. *Appl. Phys. Lett.* **85**(17), 3792 (2004)
19. E. Cartier, J.H. Stathis, D.A. Buchanan, Passivation and depassivation of silicon dangling bonds at the Si/SiO₂ interface by atomic hydrogen. *Appl. Phys. A* **63**(1510), 2 (1993)
20. A. Stesmans, Interaction of Pb defects at the (111) Si/SiO₂ interface with molecular hydrogen: simultaneous action of passivation and dissociation. *J. Appl. Phys.* **88**(1), 489 (2000)
21. A.O. Sio, S. Li, N. Yang, X. Yuan, C. Liu, X. Ye, H. Li, Hydrogen induced interface passivation in atomic layer deposited Al₂O₃ films and Al₂O₃/SiO₂ stacks. *Mater. Sci. Semicond. Process.* **83**, 171 (2018)
22. G. Dingemans, W. Beyer, M.C.M. Van De Sanden, W.M.M. Kessels, Hydrogen induced passivation of Si interfaces by Al₂O₃ films and SiO₂/Al₂O₃ stacks. *Appl. Phys. Lett.* **97**(15), 1–3 (2010)
23. B. Hoex, J.J.H. Gielis, M.C.M. van de Sanden, W.M.M. Kessels, On the c-Si surface passivation mechanism by the negative-charge-dielectric Al₂O₃. *J. Appl. Phys.* **104**(11), 1–7 (2008)
24. G. Dingemans, M.C.M. Van De Sanden, W.M.M. Kessels, Influence of the deposition temperature on the c-Si surface passivation by Al₂O₃ films synthesized by ALD and PECVD. *Electrochem. Solid State Lett.* **13**(3), H76 (2010)
25. G. Dingemans, R. Seguin, P. Engelhart, M.C.M. van de Sanden, W.M.M. Kessels, Silicon surface passivation by ultrathin Al₂O₃ films synthesized by thermal and plasma atomic layer deposition. *Phys. status solidi Rapid Res. Lett.* **4**(1–2), 10 (2010)
26. R. Zhang, J.C. Lin, X. Yu, M. Takenaka, S. Takagi, Impact of plasma post oxidation temperature on interface trap density and roughness at GeO_x/Ge interfaces. *Microelectron. Eng.* **109**, 97 (2013)
27. A. Delabie, A. Alian, F. Bellenger, M. Caymax, T. Conard, A. Franquet, S. Sioncke, S. Van Elshocht, M.M. Heyns, M. Meuris, H₂O- and O₃-based atomic layer deposition of high-κ dielectric films on GeO₂ passivation layers. *J. Electrochem. Soc.* **156**(10), G163 (2009)
28. R. Zhang, P.-C. Huang, J.-C. Lin, M. Takenaka, S. Takagi, Atomic layer-by-layer oxidation of Ge (100) and (111) surfaces by plasma post oxidation of Al₂O₃/Ge structures. *Appl. Phys. A* **102**, 1–4 (2013)
29. M. Ke, M. Takenaka, S. Takagi, Slow trap properties and generation in Al₂O₃/GeO_x/Ge MOS interfaces formed by plasma oxidation process. *ACS Appl. Electron Mater.* **1**, 311 (2019)
30. L. Zhang, H. Li, Y. Guo, K. Tang, J. Woicik, J. Robertson, P.C. McIntyre, Selective passivation of GeO₂/Ge interface defects in atomic layer deposited high-κ MOS structures. *Appl. Mater. Interfaces* **7**, 20499–20506 (2015)
31. M. Botzakaki, A. Kerasidou, L. Sygellou, V. Ioannou-Sougleridis, N. Xanthopoulos, S. Kennou, S. Ladas, N.Z. Vouroutzis, T. Speliotis, D. Skarlatos, Interfacial properties of ALD-deposited Al₂O₃/p-type germanium MOS structures: influence of oxidized Ge interfacial layer dependent on Al₂O₃ thickness. *ECS Solid State Lett.* **1**(2), P32 (2012)
32. X. Li, A. Li, X. Liu, Y. Gong, X. Chen, H. Li, D. Wu, Effect of chemical surface treatments on interfacial and electrical characteristics of atomic-layer-deposited Al₂O₃ films on Ge substrates. *Appl. Surf. Sci.* **257**(10), 4589 (2011)
33. K. Kita, S. Suzuki, H. Nomura, T. Takahashi, T. Nishimura, A. Toriumi, Direct evidence of GeO volatilization from GeO₂/Ge and impact of its suppression on GeO₂/Ge metal–insulator–semiconductor characteristics. *Jpn. J. Appl. Phys.* **47**(4), 2349 (2008)
34. K. Prabhakaran, F. Maeda, Y. Watanabe, T. Ogino, Distinctly different thermal decomposition pathways of ultrathin oxide layer on Ge and Si surfaces. *Appl. Phys. Lett.* **76**(16), 2244 (2000)
35. D. Kuzum, T. Krishnamohan, A.J. Pethe, A.K. Okyay, Y. Oshima, Y. Sun, J.P. McVittie, P.A. Pianetta, P.C. McIntyre, K.C. Saraswat, Ge-interface engineering with ozone oxidation for low interface-state density. *IEEE Electron Device Lett.* **29**(4), 328 (2008)
36. T. Hanrath, B.A. Korgel, Chemical surface passivation of Ge nanowires. *J. Am. Chem. Soc.* **126**(47), 15466 (2004)
37. M. Houssa, G. Pourtois, V.V. Afanas, A. Stesmans, First-principles study of Ge dangling bonds in GeO₂ and correlation with electron spin resonance at Ge/GeO₂ interfaces. *Appl. Phys. Lett.* **99**, 1–3 (2012)
38. Y. Fukuda, T. Ueno, S. Hirono, S. Hashimoto, Electrical characterization of germanium oxide/germanium interface prepared by electron-cyclotron-resonance plasma irradiation. *Jpn. J. Appl. Phys.* **44**, 6981 (2005)
39. Y. Fukuda, S. Member, Y. Yazaki, Y. Otani, T. Sato, H. Toyota, T. Ono, Low-temperature formation of high-quality GeO₂ interlayer for high-κ gate dielectrics/Ge by electron-cyclotron-resonance plasma techniques. *IEEE Trans. Electron Devices* **57**(1), 282 (2010)
40. H. Matsubara, T. Sasada, M. Takenaka, S. Takagi, Evidence of low interface trap density in GeO₂/Ge metal–oxide–semiconductor structures fabricated by thermal oxidation. *Appl. Phys. Lett.* **93**(3), 1–3 (2008)
41. N.M. Terlinden, G. Dingemans, M.C. van de Sanden, W.M.M. Kessels, Role of field-effect on c-Si surface passivation by ultrathin (2–20 nm) atomic layer deposited Al₂O₃. *Appl. Phys. Lett.* **96**, 112101 (2010)

42. J. Kang, R. Zhang, M. Takenaka, S. Takagi, Suppression of dark current in GeO_x-passivated germanium metal–semiconductor–metal photodetector by plasma post-oxidation. *Opt. Express* **23**(13), 16967 (2015)
43. W. Fussel, M. Schmidt, H. Angermann, G. Mende, Defects at the Si/SiO₂ interface: their nature and behaviour in technological processes and stress. *Nucl. Instrum. Methods Phys. Res. A* **377**(2–3), 177 (1996)
44. G. Dingemans, F. Einsele, W. Beyer, M.C.M. Van De Sanden, W.M.M. Kessels, Influence of annealing and Al₂O₃ properties on the hydrogen-induced passivation of the Si/SiO₂ interface. *J. Appl. Phys.* **111**, 093713 (2012)
45. H. Profijt, S.E. Potts, M.C.M. Sanden, W.M.M. Kessels, Plasma-assisted atomic layer deposition: basics, opportunities, and challenges. *J. Vac. Sci. Technol. A* **29**, 050801 (2011)
46. F. Werner, B. Veith, D. Zielke, L. Kuhnemund, T. Christoph, M. Seibt, R. Brendel, J. Schmidt, Electronic and chemical properties of the c-Si/Al₂O₃ interface. *J. Appl. Phys.* **109**, 1–5 (2011)
47. G. Dingemans, Nanolayer Surface Passivation Schemes for Silicon Solar Cells, Doctoral Thesis, Eindhoven University of Technology, 2011
48. R. Zhang, T. Iwasaki, N. Taoka, M. Takenaka, S. Takagi, Al₂O₃/GeO_x/Ge gate stacks with low interface trap density fabricated by electron cyclotron resonance plasma postoxidation. *Appl. Phys. Lett.* **98**(11), 1–3 (2011)
49. F. Werner, B. Veith, D. Zielke, L. Kuhnemund, C. Tegenkamp, M. Seibt, J. Schmidt, R. Brendel: Improved understanding of recombination at the Si/Al₂O₃ interface. In *25th European Photovoltaic Solar Energy Conference and Exhibition*, Valencia, Spain, 2010, pp. 1121–1124
50. H. Angermann, T. Dittrich, H. Flietner, Investigation of native-oxide growth on HF-treated Si(III) surfaces by measuring the surface-state distribution. *Appl. Phys. A* **59**, 193 (1994)
51. H. Angermann, W. Henrion, A. Roseler, Wet-chemical conditioning of silicon: electronic properties correlated with the surface morphology, in *Silicon-Based Materials and Devices*, 1st edn., ed. by H.S. Nalwa (Academic, San Diego, 2001), pp. 268–297
52. W. Fussel, M. Schmidt, H. Flietner, Radiation induced degradation of Si/SiO₂ structures and the nature of defects. *Nucl. Instrum. Methods Phys. Res. B* **65**, 238 (1992)
53. M. Houssa, G. Pourtois, M. Caymax, M. Meuris, M.M. Heyns, Electronic properties of (100)Ge/Ge(Hf)O₂ interfaces: a first-principles study. *Surf. Sci.* **602**(4), L25 (2008)
54. S. Baldovino, A. Molle, M. Fanciulli, Evidence of dangling bond electrical activity at the Ge/oxide interface. *Appl. Phys. Lett.* **93**, 1–3 (2010)
55. A. Stesmans, V.V. Afanas'ev, Point defects in stacks of high-k metal oxides on Ge: contrast with the Si case. In *Advanced Gate Stacks for High-Mobility Semiconductors* (Springer, Berlin, 2007), pp. 211–228
56. V.V. Afanas, Y.G. Fedorenko, A. Stesmans, Interface traps and dangling-bond defects in (100)Ge/HfO₂. *Appl. Phys. Lett.* **87**, 1–3 (2005)
57. J.R. Weber, A. Janotti, P. Rinke, C.G. Van De Walle, Dangling-bond defects and hydrogen passivation in germanium. *Appl. Phys. Lett.* **91**, 142101 (2007)
58. A. Stesmans, T. Nguyen Hoang, V.V. Afanas'ev, Hydrogen interaction kinetics of Ge dangling bonds at the Si_{0.25}Ge_{0.75}/SiO₂ interface. *J. Appl. Phys.* **116**(4), 1–16 (2014)
59. G. Dingemans, N.M. Terlinden, D. Pierreux, H.B. Profijt, M.C.M. Van De Sanden, W.M.M. Kessels, Influence of the Oxidant on the Chemical and Field-Effect Passivation of Si by ALD Al₂O₃. *Electrochem. Solid State Lett.* (2011). <https://doi.org/10.1149/1.3501970>
60. B. Hoex, J. Schmidt, P. Pohl, M.C.M. van de Sanden, W.M.M. Kessels, Silicon surface passivation by atomic layer deposited Al₂O₃. *J. Appl. Phys.* **104**(4), 1–11 (2008)
61. J.J.H. Gielis, B. Hoex, M.C.M. Van De Sanden, W.M.M. Kessels, Negative charge and charging dynamics in Al₂O₃ films on Si characterized by second-harmonic generation. *J. Appl. Phys.* **104**(7), 1–5 (2008)
62. X. Wang, J. Xiang, C. Zhao, T. Ye, W. Wang, Oxidation mechanism and surface passivation of germanium by ozone. *IEEE Electron Devices Technol. Manuf. Conf. Proc. Tech. Pap.* **60**(2013), 162 (2017)
63. S.B.S. Heil, J.L. van Hemmen, C.J. Hodson, N. Singh, F. Roozeboom, J.H. Klootwijk, M.C.M. van de Sanden, W.M.M. Kessels, Deposition of TiN and HfO₂ in a commercial 200 mm remote plasma atomic layer deposition reactor. *J. Vac. Sci. Technol. A* **25**(5), 1357 (2007)
64. M. Sinton, R.A. Cuevas, A. Stuckings, Quasi-steady-state photoconductance, a new method for solar cell material and device characterization. In *Proceedings of the 25th IEEE Photovoltaic Specialist Conference* (1996), pp. 457–460
65. E. Cornagliotti, G. Agostinelli, J. Van Der Heide, N.E. Posthuma, G. Beaucarne, J. Poortmans, Extension of QSSPC lifetime measurement to germanium samples. In *Conference Record of the 2006 IEEE 4th World Conference on Photovoltaic Energy Conversion* (IEEE, 2006), pp. 1869–1871
66. K.R. McIntosh, L.E. Black, On effective surface recombination parameters. *J. Appl. Phys.* **116**(1), 014503 (2014)
67. M. Schbftaler, R. Brendel, G. Langguth, J.H. Werner, High-quality surface passivation by corona-charged oxides for semiconductor surface characterization. In *Proceedings of 1994 IEEE 1st World Conference on Photovoltaic Energy Conversion* (1994), pp. 1509–1512
68. M.M. Mandoc, M.L.C. Adams, G. Dingemans, N.M. Terlinden, M.C.M. Van De Sanden, Corona charging and optical second-harmonic generation studies of the field-effect passivation of c-Si

- by Al₂O₃ films. In *35th IEEE Photovoltaic Specialists Conference*, Honolulu, Hawaii, United States, 2010, pp. 3200–3204
69. S.W. Glunz, D. Biro, S. Rein, W. Warta, Field-effect passivation of the SiO₂-Si interface. *J. Appl. Phys.* **86**(1), 683 (1999)
70. N. Bicais-Lépinay, F. André, R. Pantel, S. Jullian, A. Margain, L.F.T. Kwakman, Lift-out techniques coupled with advanced TEM characterization methods for electrical failure analysis. *Microelectron. Reliab.* **42**, 1747 (2002)